A New View of Cold H I Clouds in the Milky Way

Steven J. Gibson[1], A. Russell Taylor[1], Lloyd A. Higgs[2], and Peter E. Dewdney[2]

ABSTRACT

We reveal cold Galactic clouds of neutral hydrogen in unprecedented detail. Our 21cm synthesis maps, taken from the Canadian Galactic Plane Survey, show a numerous and diverse population of H I self-absorption (HISA) features in gas outside the Solar circle. These objects vary in size, shape, and contrast against the background H I. All display a high level of angular and velocity structure, and most would appear significantly diluted, if not invisible, in lower-resolution H I surveys. A number of Perseus arm features remain unresolved by the $1'$ beam of our survey, with apparent diameters < 0.6 pc at 2 kpc distance.

The majority of HISA features we detect have no obvious ^{12}CO emission counterparts. This suggests either HISA is not found predominantly in molecular clouds, as has often been presumed in the past, or CO is not a good tracer of H_2. Some HISA lacking CO shows far-infrared dust emission, though whether this arises from shielded molecular gas or diffuse atomic clouds is not clear.

Constraining the gas properties of HISA remains a difficult problem, but we introduce a new method which aids this process. Our approach relates a number of physical parameters via gas law and line integral relationships, and should prove powerful if the input variables are sufficiently well known. We explore the current allowed parameter ranges for three sample features of very different appearance. We find spin temperatures $\lesssim 50$ K and densities $\gtrsim 10^2$ cm^{-3}.

Subject headings: radiative transfer — methods: analytical — ISM: clouds — ISM: globules – ISM: structure — radio lines: ISM

1. Introduction

1.1. Charting Cold H I in the Galaxy

Cold atomic gas, with $T \lesssim 100$ K, is a major constituent of interstellar matter. Most of our knowledge of this gas is gleaned from neutral hydrogen (H I) 21cm line emission spectra or various

[1]Dept. of Physics & Astronomy, University of Calgary, 2500 University Drive N.W., Calgary, Alberta T2N 1N4, Canada; gibson@ras.ucalgary.ca; russ@ras.ucalgary.ca

[2]Dominion Radio Astrophysical Observatory, Box 248, Penticton, British Columbia V2A 6K3, Canada; Lloyd.Higgs@hia.nrc.ca; Peter.Dewdney@hia.nrc.ca

absorption studies toward continuum sources at radio and optical wavelengths (see Kulkarni & Heiles 1988 and Dickey & Lockman 1990 for reviews). H I emission maps are poor tracers of cold gas, since the H I line intensity is proportional to excitation temperature when optically thick, and is independent of temperature when optically thin (see §4). In either case, separation of the warm and cold H I emission components requires great care, even when the two are relatively distinct (e.g., Pöppel, Marronetti, & Benaglia 1994). Absorption methods, on the other hand, are hampered by the small number of bright, extended continuum background sources (e.g., W3: see Normandeau 1999 and references therein). VLBI maps against more compact sources reveal small-scale H I structure (Faison et al. 1998), but cannot chart the gas distribution over any large area. The alternative use of a grid of point sources (e.g., Na I: Meyer & Lauroesch 1999; H I: Garwood & Dickey 1989) is limited by the available source distribution and the discreteness of the angular sampling.

A direct view of the spatial structure of cold atomic gas is provided by observations of H I self-absorption (HISA) against diffuse background H I emission. Though the HISA phenomenon has been known for many years (Heeschen 1955), its full potential for mapping cold H I has remained unrealized, due to several observational and analytic difficulties. Chief among these are uncertainties in the background emission spectrum, which limit the accuracy of the estimated absorption spectrum, and inadequate constraints on the equation of radiative transfer, which complicate the extraction of physical parameters. As a result, the properties, distribution, behavior, and environment of HISA gas are not well understood.

Several problems are diminished by the use of higher angular resolution, which allows brightness measurements closer to HISA feature edges for improved background spectrum estimation, as well as reduced beam dilution effects and a more detailed view of cloud structure. Despite these advantages, few synthesis imaging studies of HISA (van der Werf, Goss, & Vanden Bout 1988; van der Werf et al. 1989; Feldt & Wendker 1993; Feldt 1993) have been made, primarily because of the large effort required to map such clouds interferometrically over any significant area. Our new survey (§1.3) seeks to rectify this shortcoming. As might be expected for cold H I, we find many small, faint features which a single dish survey would miss.

1.2. Environmental Context

Of equal importance to the need for high angular resolution is the need for broad sky coverage. The physical relationships between HISA and other interstellar constituents like dust and H_2 are difficult to investigate without the benefit of large scale, unbiased surveys. HISA studies to date have taken one of two forms: targeted surveys of known dark clouds, or limited explorations in the vicinity of the Galactic plane, both with single dish instruments.

The highest resolution surveys have employed the $3'$ beam of the Arecibo telescope to examine selected strips of sky (Baker & Burton 1979) or partially sampled maps (Bania & Lockman 1984).

These are restricted to portions of the Galactic plane observable with that facility, mostly in the inner Galaxy. Comparisons of the Arecibo data with CO emission (Burton, Liszt, & Baker 1978; Liszt, Burton, & Bania 1981; Peters & Bash 1987; Jacq, Baudry, & Walmsley 1988) show correlations between HISA and molecular gas which are significant, but far from absolute (e.g., Peters & Bash 1987). Instead, CO and HISA are each found separately as well as together, implying H_2 and HISA are frequently independent, unless the CO is not tracing the H_2 in this case. Sensitivity limitations as well as confusion in identifying many HISA features may cause the HISA-CO association to appear more limited than it actually is, but caution suggests seeking more evidence before asserting a stronger relationship. At the least, some cold H I will not be visible as HISA due to unfavorable viewing geometry.

Likewise, targeted studies of individual clouds do not demonstrate unambiguous relations between interstellar constituents. Dark cloud surveys (e.g., Knapp 1974; McCutcheon, Shuter, & Booth 1978) find many dusty objects with no detected HISA; the reverse case of HISA without dust is not testable with such preselected samples. Even within clouds containing both HISA and molecular gas, the HISA/molecular ratio does not behave consistently, but instead is found to rise toward the cloud cores in some cases (Hasegawa, Sato, & Fukui 1983) and to fall in others (Feldt 1993), leaving the relationship between these gas phases unclear. Detailed examinations of many clouds are necessary to determine what physical relations between HISA, H_2 and other ISM components predominate, as well as the role of environmental factors like the local radiation field. Our new survey's high angular resolution and broad sky coverage enable us to address these issues objectively.

1.3. This Work

In this paper, we present initial results from a large scale, high resolution survey of HISA in the *outer* Galaxy, undertaken with data from the ongoing Canadian Galactic Plane Survey (CGPS; Taylor et al. 2000). We are mapping cold Galactic H I clouds at $\sim 1'$ resolution over the coordinate range $147.3^\circ > \ell > 74.2^\circ$, $-3.6^\circ < b < +5.6^\circ$. The unprecedented angular coverage and detail of the CGPS allow us to address a number of the observational concerns listed above. Relations between HISA and other ISM constituents are revealed by comparison with maps of dust and CO emission. Our use of sightlines beyond the Solar circle reduces the velocity-distance ambiguities inherent in inner Galaxy studies, simplifying issues of radiative transfer. We introduce additional constraints on radiative transfer parameters which, under suitable conditions, permit the direct extraction of physical properties of the HISA gas.

We begin with a brief description of the CGPS data (§2), followed by an overview of detected HISA features (§3). We then outline our analysis technique (§4) and discuss derived properties (§5). A thorough census of HISA features in our survey, discussions of global properties, and other issues will be presented in subsequent papers.

2. Survey Data

For convenience, we list a few aspects of the Canadian Galactic Plane Survey of immediate relevance to our study. Readers interested in more details are encouraged to consult Taylor et al. (2000).

As noted in §1.3, the CGPS covers a $73^\circ \times 9^\circ$ region along the Milky Way visible from the northern hemisphere, roughly from Perseus through Cygnus. Observations are being made with the Synthesis Telescope, a 7-element east-west interferometric array at the Dominion Radio Astrophysical Observatory near Penticton, British Columbia Landecker et al. (1999). The survey area is mapped in 21cm line and continuum and 74cm continuum emission as a mosaic of 38×5 synthesis fields on a hexagonal grid, with field separations equal to 1.04 primary beam full widths at half maximum (FWHM) at 21cm. Short spacing data are provided by a parallel survey with the DRAO 26m telescope for H I 21cm spectra and by other surveys for the continuum bands. The combined synthesis and single dish data give complete *uv* coverage of all spatial frequencies up to the inverse width of the synthesized beam. This is essential for adequate detection of multiscale structure in the gas.

The DRAO-ST beam FWHM is $1' \times 1' \mathrm{cosec}(\delta)$ at 21cm. The instrumental velocity resolution of 1.319 $\mathrm{km\,s^{-1}}$ is sampled every 0.824 $\mathrm{km\,s^{-1}}$; the narrowest measurable features have widths of ≥ 2 channels, or 1.65 $\mathrm{km\,s^{-1}}$. The velocity coverage of -155 to $+45$ $\mathrm{km\,s^{-1}}$ encompasses all significant Galactic H I emission in this area of the sky.

The 21cm primary beam FWHM is $107'$, with a synthesis field cutoff radius at 10% of field center sensitivity, corresponding to $r = 93'$. Though only 21cm line maps are shown in this paper, we use 21cm continuum measurements as part of our estimation of background brightness in the radiative transfer equation (§4). The field-center sensitivities in the data we present in this paper are $1\sigma \lesssim 0.07$ K in 21cm continuum and $3 - 6$ K in individual H I channels, depending on whether the primary beam is empty or filled with bright H I emission; noise between field centers can be up to 1.6 times higher.

In addition to the DRAO data, we employ maps of dust grain far-IR thermal emission from *IRAS* HIRES data (Cao et al. 1997) and FCRAO ^{12}CO $J = 1 \rightarrow 0$ spectral line survey data (Heyer et al. 1998) to compare spatial distributions of HISA with those of dust and molecular gas. These parallel survey data have angular resolutions of 1-2$'$, with a CO spectral resolution similar to the DRAO H I.

3. HISA Features

3.1. Identification

The process of identifying HISA features consists of first locating apparent minima in H I 21cm emission maps or spectra, and then demonstrating that these minima result from self-absorption rather than a mere absence of emission.

HISA confirmation criteria have been discussed by a number of authors (e.g., Knapp 1974; Baker & Burton 1979). Briefly, these criteria seek to dismiss an emission hole as a viable explanation, leaving HISA as the remaining option. They require: (1) line FWHM of only a few $\mathrm{km\,s^{-1}}$, narrower than nearly all observed emission features (see Goerigk et al. 1983 for an exception); (2) wings steeper than can be replicated by a conspiracy of neighboring emission lines, which rarely exhibit such slopes in isolation; and (3) a greater amount of small-scale angular structure than is seen in emission clouds, especially those providing background illumination.

By themselves, these conditions are insufficient, since all three are met by occasional H I emission features in isolation, either away from the Galactic plane or at interarm gas velocities. A cursory inspection of the CGPS H I data turns up a number of small-scale, narrow-velocity emission clouds, which typically have brightness amplitudes of $\sim$20 K or less. However, we do not find any of these features against H I backgrounds brighter than a few tens of Kelvins. Perhaps they do not occur at these higher column densities, or perhaps they become blended and lost in the general H I "soup". Whatever the physical situation, the first three criteria are strengthened by a fourth requiring a minimum H I background level, since this keeps gaps between small-scale or narrow-velocity emission features at low column density from being mistaken for self-absorption. The HISA clouds we discuss in this paper all have backgrounds in excess of 80 K.

Cold H I clouds identified with these strict criteria are subject to three selection biases: the need for favorable viewing geometry to produce self-absorption, the need for the self-absorption to be sufficiently compact to distinguish it from emission gaps, and the need for relatively high H I column density. In the spatial domain, the population of identifiable HISA clouds is confined to the Galactic plane, and to narrow or compact self-absorption features occurring primarily on scales where the angular power spectrum of the background H I is weak. In the velocity domain, only features with bright H I backgrounds and low dispersions are trustworthy. The latter is not a temperature constraint, though HISA gas *is* required to be cooler than the background by radiative transfer (see §4). Instead, it is a constraint on total linewidth. Most cool H I lines are dominated by nonthermal broadening, such as turbulence. As a result, only the most *quiescent* HISA can be identified, and more turbulent features will be missed. These selection effects serve as sober reminders of how incomplete any HISA census of cold H I may be.

One additional HISA identification criterion often used is to require matching molecular emission or the presence of dust (Knapp 1974). Since HISA has been found without such features (§1.2), requiring them represents an extra source of bias which should be avoided.

Below, we discuss the appearance of HISA features in the CGPS, identifying the local H I minima visually in channel maps and choosing those satisfying the strict HISA criteria above. We have made these selections to illustrate several traits of interest. A future HISA population study will employ an automated detection algorithm to ensure an objective sample.

3.2. Overview of Features

Fig. 1 shows a large area of the currently mapped H I survey at a radial velocity of -41 km s^{-1} with respect to the Local Standard of Rest, the reference frame we adopt for all velocities hereafter (see, e.g., Mihalas & Binney 1981). Gas with this velocity is located in the Perseus arm of the Galaxy at a distance of order 2 kpc, and may be participating in streaming motions associated with a spiral density wave (Roberts 1972).

A considerable amount of structural detail is apparent in the H I emission in Fig. 1. The field is filled with overlapping knots, filaments, and other complex shapes, some with associated CO emission, as indicated by contours from the Heyer et al. (1998) survey. In addition, quite a few dark, sinuous HISA features are visible at varying amounts of contrast with the background; many are on the edge of discernability. HISA is most common in areas where the background brightness temperature exceeds ~ 100 K, but is especially prominent near $\ell = 140°$, $b = +1°$. While a few features are clearly associated with molecular gas, many have no apparent CO counterparts, despite their morphological similarity to molecular clouds. Since CO features exist in the FCRAO survey down to its 0.6 K rms limit, and line intensities several times lower have been observed (Allen & Lequeux 1993), we cannot rule out some HISA features being associated with faint, undetected molecular emission. Alternatively, H_2 may be present without CO, as has been inferred for a number of clouds with an apparent excess of dust emission relative to H I and CO (Reach et al. 1994; Meyerdierks & Heithausen 1996). But independent of these issues, the available data prohibit any simple proportional relationship between the darkness of HISA and brightness of CO for most features. We will discuss the HISA-CO relation quantitatively with a HISA census in a subsequent paper.

Fig. 1 shows only one velocity channel; a "movie" of many channels in sequence reveals the kinematics of these features, plus a large number of others occurring at different velocities. Due to its narrow linewidths, the HISA changes rapidly with velocity. Individual clouds appear briefly for intervals of only a few km s^{-1}, and some may be spectrally unresolved in our data. Often small velocity gradients are exhibited within features, and somewhat larger gradients extend over major HISA complexes. On the largest angular scales, a HISA longitude-velocity trend is evident which seems to follow the same general Galactic rotation law as the H I emission. This behavior is partly expected from selection effects (§3.1), but is also consistent with HISA tracing some aspect of spiral arm structure.

3.3. Sample Objects

We examine three sample features in detail, to demonstrate their reality as HISA and to explore their general characteristics. The physical properties of these objects are analyzed in §5.

The examples are selected to illustrate a wide range of feature parameter space. HISA with both 60 μm dust and ^{12}CO emission, with dust but without CO, and without dust but with possible CO are given. We present HISA with a variety of morphologies, velocity structures, and ON-OFF intensity contrasts, in both the Local and Perseus arms.

3.3.1. Extended Perseus Complex

Fig. 2 shows an enlargement of one area in Fig. 1 where a relatively strong association exists between HISA and CO. Many of the same features also contain significant dust emission, as revealed by the 60 μm intensity contours. But even here, HISA features are visible without CO or dust, or with only one of the two. For a Perseus arm distance of 2.0 kpc, the map scale is 0.58 pc arcmin^{-1}.

We have extracted H I and CO spectra for two features we label as "complex" and "globule" in Fig. 2 and have plotted them in Fig. 4. The former is one piece of a large HISA complex extending over much of Fig. 2, whose boundaries are somewhat difficult to define objectively. The latter is an unresolved knot on the periphery of this feature, and is discussed separately below (§3.3.2). All spectra are taken from averages over the boxes in Fig. 2 to improve S/N except the globule's ON spectrum, which is from a solitary sightline. Both features display prominent self-absorption troughs at -41 km s^{-1}. The large displacement of the complex's OFF extraction area is necessary to ensure it is free of HISA. The cost of this larger angular separation is greater ON-OFF spectral disagreement for this feature than for the others in Fig. 4; most of the other features' discrepancies are noise-related.

The complex's HISA spectrum shows a full linewidth at half maximum of $\sim$4.5 km s^{-1}, which is narrow for emission components of cold neutral gas, but not unknown (e.g., Pöppel et al. 1994). If we base our evaluation solely on this spectrum, the possibility of the feature arising from an emission trough rather than HISA exists (§3.1). But this is an average over all the structure within the box. When the different sightlines within the box are examined separately, considerable variation in line shape and depth is revealed; at some positions, linewidths are $2-3$ km s^{-1}, which can only arise from HISA. This indicates that other sightlines, as well as the average spectrum, probably show a blend of several such narrow components, a view consistent with the large amount of spatial substructure in the image.

3.3.2. Dark, Unresolved Globule

The globular feature bracketed by the two small black boxes in Fig. 2 is a particularly strong, narrow, and isolated example of the sort of substructure which may appear blended together within the larger HISA complex. This compact feature has a velocity width of $\sim$2.5 km s^{-1} (Fig. 4) and is unresolved by the 1′ DRAO beam. As a result, its line FWHM and projected diameter of $\sim$0.6 pc are upper limits, and its apparent optical depth is diluted from the true value. The globule shows dust emission but no CO; the latter may result from a sensitivity limitation. We find a number of dark, unresolved blobs of this sort in the CGPS H I data, several more of which are visible in Fig. 2. While H I absorption against a compact continuum source can produce a similar spatial appearance, most of these features, including our selected globule, have no such background source. The absorption amplitudes of these unresolved features cover a wide range, from several tens of Kelvins down to the noise limit. This one is among the strongest, with a contrast at line center exceeding 60 K.

3.3.3. Faint Local Filament

HISA is also visible in gas at Local velocities, though it is generally fainter than HISA in the Perseus arm. Since the Local H I background is typically $\gtrsim$ 30 K fainter than the Perseus H I background, features of similar optical depth and spin temperature will appear weaker locally (see §4). This effect accounts at least partly for the dearth of Local HISA, but the Local arm may also simply contain less cold H I.

One of the most prominent, though still weak, Local HISA features is shown in the 0 km s^{-1} channel map in Fig. 3, and spectrally in Fig. 4. Like the Perseus globule, it has a velocity width of 2.5 km s^{-1}, but its contrast against the background H I is only $\sim$15 K. No corresponding dust emission is found at this location. The feature unfortunately lies outside the longitude coverage of the Heyer et al. (1998) CO survey. The large-scale Dame et al. (1987) survey shows marginal CO emission at this velocity, but its low spatial resolution precludes a clear match.

This HISA displays structure down to the 1′ beam, with a visible extent of only a few beams. Assuming it lies outside the Local Bubble, the feature's distance is $\geq$ 100 pc, and the image scale is $\geq$ 0.03 pc arcmin^{-1}; better distance constraints may be obtained in the future with interstellar absorption line measurements. Clearly in this case and the others above, HISA shows strong evidence for considerable fine-scale structure. While small-scale H I features have been found previously (see Heiles 1997 for a review), most have been studied via absorption toward continuum sources, which has mapping limitations (§1.1). Synthesis imaging surveys of HISA introduce a new method of probing the structural properties of interstellar gas.

4. Analysis

4.1. Radiative Transfer Considerations

In brightness temperature terms, the radiative transfer equation $dT_B/d\tau = T_B - T_S$ for H I 21cm radiation has the general solution

$$T_B \;=\; \int_0^{\tau_M} T_S(\tau)\, e^{-\tau} d\tau \;+\; T_M\, e^{-\tau_M} \quad , \tag{1}$$

where τ is the optical depth measured from zero at the observer's position out to some maximum τ_M, T_B is the observed brightness temperature, T_M is the brightness temperature at τ_M, and T_S is the spin or excitation temperature of the H I gas. For clarity, the velocity dependencies of brightness temperatures and optical depths are not shown.

The integral form of the radiative transfer solution cannot be used directly, but can be rewritten in terms of discrete, isothermal components. Many classical HISA studies have employed the simple two-component case,

$$T_B \;=\; T_S \left(1 - e^{-\tau}\right) \;+\; T_M\, e^{-\tau} \quad , \tag{2}$$

where self-absorption occurs if $T_S < T_M$. A more realistic treatment considers four components: foreground H I emission, midground HISA, background H I emission, and a continuum emission component represented as lying in the far background for simplicity. These are illustrated in Fig. 5, and manifest as

$$\begin{aligned} T_B \;=\;& [T_S]_{fg} \left(1 - e^{-\tau_{fg}}\right) \;+\; [T_S]_{HISA} \left(1 - e^{-\tau_{HISA}}\right) e^{-\tau_{fg}} \\ & +\; [T_S]_{bg} \left(1 - e^{-\tau_{bg}}\right) e^{-\left(\tau_{fg} + \tau_{HISA}\right)} \;+\; T_C\, e^{-\left(\tau_{fg} + \tau_{HISA} + \tau_{bg}\right)} \quad , \end{aligned} \tag{3}$$

where T_M has been replaced with the out-of-band continuum brightness T_C, and T_S and τ with the spin temperature and optical depth for each H I component. It is important to remember these T_S and τ values are functions of radial velocity v; all H I clouds represented here must share the same v to participate in the radiative transfer.

Since HISA distinguishable from emission gaps occurs predominantly on smaller angular scales than H I emission bright enough to serve as an adequate background (§3.1), in the most likely scenario, lines of sight adjacent to the HISA will intersect the two H I emission clouds (Fig. 5). Alternative geometries are possible in which the emission clouds are less extensive than the HISA host cloud, only part of which will then self-absorb. However, the lack of features in our survey which appear to change from HISA to H I emission across a changing background indicates this

scenario is relatively uncommon. We assume the small-cloud HISA model, for which the OFF-HISA brightness temperature is found by setting $\tau_{HISA} = 0$ in Equation (3). The difference between ON and OFF observed intensities is then

$$T_{ON} - T_{OFF} = \left([T_S]_{HISA} - p\,T_{OFF} - T_C e^{-\tau_{bg}} \right) e^{-\tau_{fg}} \left(1 - e^{-\tau_{HISA}} \right) \quad , \tag{4}$$

where $p \equiv [T_S]_{bg}(1 - e^{-\tau_{bg}})/T_{OFF}$, and we have defined T_{ON} and T_{OFF} as observed intensities from which the continuum background T_C has been subtracted, the standard practice in H I spectral line reduction. In this representation, self-absorption is obtained when $T_{ON} < T_{OFF}$.

A final adjustment is to let τ_{bg} and τ_{fg} be small, which reduces our representation to Feldt's (1993):

$$T_{ON} - T_{OFF} = (T_S - T_C - p\,T_{OFF}) \left(1 - e^{-\tau} \right) \quad . \tag{5}$$

Here the remaining free parameters are $\tau = \tau_{HISA}$, $T_S = [T_S]_{HISA}$, and p, which now represents the fraction of H I emission originating behind the HISA cloud. We use this form in our analyses.

Is it reasonable to assume τ_{bg} and τ_{fg} are negligible? If, as we have suggested in §1, the H I brightness is dominated by warm neutral gas, with a kinetic temperature $T_K \sim 8000\ K$, then low values of τ_{bg} and τ_{fg} are required to produce the brightness temperatures we observe in the CGPS, which are generally $\lesssim 150$ K. Possible difference factors of a few between the kinetic temperature and spin temperature for warm neutral gas (Kulkarni & Heiles 1988) are not enough to allow opaque gas in this case.

The alternative of cooler, higher-τ gas dominating the H I brightness cannot be ruled out, but some limits apply. In most areas of our survey, we find $T_C \ll T_B$, so the errors from assuming a small τ_{bg} are minimal. A significant τ_{fg} produces a global rescaling, which acts to increase T_S and τ_{HISA}, or to decrease p. However, in a survey such as ours, the HISA features which are easiest to identify are likely to have the bulk of the H I behind them, since that viewing geometry is more favorable. This selection bias increases the probability that τ_{fg} is low for most detectable features. If it is high instead, our estimates of the amount of HISA gas may become lower limits, a circumstance which is already likely if low-contrast features are common.

4.2. Methods of Constraint

The radiative transfer solution (Eq. [5]) must be constrained in order to extract estimates of physical parameters for HISA clouds in our survey. One fundamental limit is placed on each of T_S, τ, and p by Equation (5), regardless of whether $T_{ON} < T_{OFF}$. The optical depth solution

$$\tau \;=\; -\ln\left(1 \;-\; \frac{T_{ON} \;-\; T_{OFF}}{T_S \;-\; T_C - p\,T_{OFF}}\right) \tag{6}$$

is minimized for $T_S = 0$ and $p = 1$. At the other extreme, letting $\tau \to \infty$ in Equation (5) yields the limiting cases $(T_S)_{max} = T_C + T_{ON} + (p-1)\,T_{OFF}$ and $p_{min} = 1 + (T_S - T_C - T_{ON})/T_{OFF}$. These three absolute constraints are sometimes useful, but are generally not very strict.

Tighter constraints on p require detailed sightline knowledge which is difficult to come by. Since the $p = 1$ case is the most efficient for producing prominent absorption, the majority of detected HISA clouds should have values in this regime, though p remains unknown for any particular object. Means of limiting p via other parameter values will be discussed below, after considering constraints on T_S and τ.

4.2.1. Previous Methods

Several methods of constraining T_S or τ have been used or discussed by previous authors.

1. A value for T_S may be assumed. This can be a spin temperature determined for other H I gas in the vicinity of the HISA feature in question if its equivalence to the absorbing gas is compelling, or simply a "canonical" value for interstellar gas of the type found in the HISA cloud. The current state of knowledge is inadequate for the second approach. But for a subset of HISA features, T_S may be measurable in H I absorption toward serendipitous background continuum point sources (Wendker & Wrigge 1996).

2. Similarly, T_S may be constrained by observations of molecular species located with the HISA. The spin and kinetic temperatures of cold H I are closely coupled (Kulkarni & Heiles 1988), allowing T_S to be determined for HISA occurring within a molecular cloud if T_K is obtained from molecular line emission measurements, provided the H I and H_2 are in equilibrium; if not, the limit $[T_K]_{HISA} \geq [T_K]_{H_2}$ probably still applies. Yet as we have seen above, HISA frequently appears without apparent molecular counterparts, and even when the two coincide, their degree of mixing may be difficult to assess.

3. For quiescent gas, resolved HISA linewidths yield T_K, hence T_S, directly as $T_K = (\Delta v/\,0.215)^2$, where Δv is the full width at half maximum in $\mathrm{km\,s^{-1}}$, and the line shape is assumed to be Gaussian (Spitzer 1978). In some cases, this measurement is reasonable (e.g., Montgomery, Bates, & Davies 1995), but more frequently, turbulent broadening reduces it to an upper limit for T_K, and not an especially interesting one.

4. T_S may also be measured directly from a feature which changes from HISA to H I emission against a diminishing background. In the transition area $T_{ON} = T_{OFF}$, and Equation (5) gives

$T_S = T_C + p\,T_{OFF}$. However straightforward, this approach requires HISA features with convincing transitions to emission. Such clouds are known (Bania & Lockman 1984; Montgomery et al. 1995), but appear to be uncommon; we have not found satisfactory candidates at this stage of our survey.

5. Finally, under suitable conditions, line *shape* yields τ directly, both for H I emission (Rohlfs, Braunsfurth, & Mebold 1972) and for self-absorption (Levinson & Brown 1980). For a Gaussian or similar profile, the line core will become increasingly flattened as $\tau \rightarrow \infty$; this presumes the line has only one velocity component. Unfortunately, the S/N required for even a moderately accurate determination of τ is much higher than that of most HISA studies (Levinson & Brown 1980), including ours. Nevertheless, we *can* rule out overly large optical depths for a Gaussian line profile, even in the presence of noise (§5).

4.2.2. New Approach

None of the above methods is particularly suited to our CGPS HISA data. An additional approach which applies some simple assumptions about the nature of the gas and its sightline distribution has not, to the best of our knowledge, been tried previously. We invoke three conditions: (1) the HISA feature must contain only one velocity component; (2) the feature must be isothermal along the line of sight; and (3) its volume density and kinetic temperature must be related via an ideal gas law.

The first two conditions enable the relation

$$\tau_0 \;=\; \frac{C\,N_{HISA}}{T_S\,\Delta v} \;=\; \frac{C}{T_S\,\Delta v}\int\limits_{\Delta s} n_{HISA}\,ds \;\;, \tag{7}$$

where τ_0 is the line center opacity, N_{HISA} and n_{HISA} are column and volume densities respectively, Δv is the full line width at half amplitude, s is the sightline path variable integrated through the HISA feature, which has thickness Δs, and the constant C is a function of line profile shape. For a Gaussian H I 21cm line, $C = 5.2\times10^{-19}\,\mathrm{cm^2\,K\,km\,s^{-1}}$ (Dickey & Lockman 1990).

The third, ideal gas condition is

$$P \;=\; n_{tot}\,k\,T_K \;\simeq\; \frac{n_{HISA}\,k\,T_S}{f_n} \;\;, \tag{8}$$

where $T_S \simeq T_K$ (§4.2.1), P/k is the gas thermal pressure in $[\,\mathrm{K\,cm^{-3}}]$, n_{tot} is the total gas density, and $f_n \equiv n_{HISA}/n_{tot}$ is the fraction of particle density contributed by the HISA gas. For an isothermal cloud of pure, neutral hydrogen gas, $f_n = n_{\rm HI}/(n_{\rm HI} + n_{\rm H_2})$. This is *not* the H I mass fraction $f_M \equiv n_{\rm HI}/(n_{\rm HI} + 2\,n_{\rm H_2})$, but can be converted as $f_M = f_n/(2 - f_n)$. Combining Equations (7) and (8) yields

$$T_S \;=\; \sqrt{\frac{\langle P \rangle \, f_n \, C \, \Delta s}{k \, \tau_0 \, \Delta v}} \;\; , \tag{9}$$

where the pressure term has been averaged over the feature's sightline dimension Δs. Ideally, lines of carbon or some other pressure tracer should be observed in the object in question to constrain $\langle P \rangle$. Absent such measurements, the next best approach is to adopt a canonical ISM thermal pressure value, errors in which are reduced by the square root in Equation (9).

Given measured or assumed values for the other variables, T_S and τ are left as unknowns in Equation (9), which can be solved numerically in combination with Equation (6). From T_S and τ we calculate N_{HISA}, n_{HISA}, and mass M_{HISA}, with the last dependent upon a distance estimate.

4.2.3. Uncertainties in the New Approach

Though free of the difficulties listed in §4.2.1, this new constraining technique is subject to its own uncertainties, both from input assumptions and parameter values.

Of the former, the presence of a single velocity component, though not universal (§3.3.1), is still common, and many multicomponent features may be sufficiently blended to treat as single components with minimal error. The implicit role of isothermality in the discrete radiative transfer formulation (§4.1) makes it unavoidable in any practical HISA analysis; if T_S does vary within the HISA cloud, the temperature treated by the discrete approach is a weighted average (Eq. [1]). Finally, the validity of the ideal gas assumption relies upon the kinetic temperature being unaffected by such nonthermal pressure sources as turbulence and magnetic fields. Neither mechanism is well understood. Nevertheless, the inequality of thermal and turbulent pressures (Heiles 1997) suggests a lack of equipartition, hence no efficient means for turbulent energy to dissipate as heat. Various mechanisms for doing the same with magnetic fields require significantly nonequilibrium conditions, which we assume here are unlikely in the general interstellar medium, though they may occur in transitory phenomena such as shocks. At least until contrary evidence appears, the ideal gas relationship should serve as a useful exploratory tool.

The constraint of input parameters is more problematic, particularly p, f_n, and Δs. Without detailed sightline information, p can best be constrained by considering its behavior in light of other parameters. Similar limits apply to f_n, but it is by far the most uncertain variable, with a potential range from 1 for pure H I clouds down to levels of 0.02 (Jacq, Baudry, & Walmsley 1988) or even less (van der Werf et al. 1988). However, values much below 1% are excluded for the HISA features we discuss (§5). The third unknown parameter is the HISA sightline pathlength Δs, which must be estimated from the appearance of the cloud on the sky. Not only do different 3-D structures appear similar in projection, e.g., cylindrical filaments and edge-on sheets, but the CGPS features also display considerable substructure, giving many possible choices for the appropriate angular

scale to relate to Δs. Fortunately, the square root in Equation (9) moderates the effects of errors Δs, f_n, and other variables. We discuss our method of selecting Δs in §5.

4.2.4. Background Estimation

One last source of uncertainty applies regardless of analysis technique: the estimation of the background spectrum, or rather, the assumption that $p\,T_{OFF}$ is representative of the brightness behind the HISA cloud. Three different background estimation techniques have been used in the past: fitting functions (Knapp 1974; McCutcheon et al. 1978) or straight lines (Hasegawa et al. 1983; Montgomery et al. 1995) across absorption features in spectra, obtaining actual T_{OFF} spectra from sightlines adjacent to the feature (Feldt 1993), or assuming a single-dish spectrum dilutes HISA features sufficiently to act as T_{OFF} (van der Werf et al. 1988). We employ the offset-spectrum method here.

5. Physical Properties

5.1. Parameter Ranges

In general, Equation (5) produces families of curves in (T_S, τ) space of the form shown in Fig. 6, with τ increasing from some minimum value at $T_S = 0$ up to infinity at $(T_S)_{max} = T_C + T_{ON} + (p-1)\,T_{OFF}$. The $p = 1$ curve is the lowest in this family, with higher curves occurring for lower p, down to the limit $p_{min} = 1 + (T_S - T_C - T_{ON})/T_{OFF}$. In practice, many of these low-p solutions require large optical depths which may be excluded if the line shape does not appear greatly saturated.

Our new method (§4.2.2) confines (T_S, τ) solutions to a subset of the curve for any particular p. The combined locus of all such curve sections is a tilted strip of slope -2 in log space. The width of the strip along the (T_S, τ) curve is determined by the amount of uncertainty in the input parameters f_n and Δs in Equation (9). For clarity, we show the effects of these two parameters separately in Fig. 6, with individual solution strips plotted for $f_n = 1.0$, 0.1, and 0.01. The lesser uncertainties in Δv, $\langle P \rangle$, and C can also affect the width, but we ignore them here, adopting a single measured value for Δv, a canonical thermal pressure of $P/k = 4000\,\mathrm{K\,cm^{-3}}$ (Kulkarni & Heiles 1988), and the Gaussian profile integral value for C (§4.2.2).

We exclude solutions with $\tau > 10$, since none of the three line profiles is consistent with an optical depth of more than a few. The cosmic microwave background constrains T_S to ≥ 2.73 K. Unless unusually weak UV radiation and cosmic ray heating allow very low temperatures, as they may in parts of M31 (Loinard & Allen 1998; Allen et al. 1995), a more reasonable HISA lower temperature limit is probably the $7 - 10$ K value found for dark molecular clouds (Wolkovitch et al. 1997; Turner 1988).

The first part of Table 1 lists the input values we have used to produce the plots in Fig. 6. Here T_{ON} and T_{OFF} refer to the line center, as does the τ derived from them. The line width Δv is measured from the difference spectrum to avoid underestimation (Levinson & Brown 1980). The solid angle Ω describes the piece of HISA being investigated. For extended objects, Ω covers only the white spectrum extraction box (see Figs. 2 & 3), *not* the entire object; derived masses for whole features must be extrapolated accordingly. For the unresolved globule however, Ω is taken as the synthesis beam.

We calculate $\Delta s = d \tan\theta_s$, where d is the distance from Earth, and θ_s is the angle corresponding to the sightline thickness of the HISA feature, i.e., its width if seen from the side. We estimate θ_s as the largest angular scale at which the feature appears "solid", which should be a reasonable gauge of the length of a random path through the object if our viewing angle is not special. For the Perseus complex feature, this scale of solidity is a few arcminutes, while for both the Perseus globule and Local filament, we have used the beam size. Since the globule is unresolved, its θ_s is an upper limit; this may also be true of the filament. Where the thickness appears resolved, as in the Perseus complex, θ_s may still be overestimated if small structures merge into larger ones in projection. As we have noted though, these uncertainties in Δs are moderated by a square root.

Finally, d itself is assigned purely on the basis of which spiral arm the gas velocity indicates. We assume the Perseus features have $d \sim 2 - 2.5$ kpc (Roberts 1972). HISA in our own arm is probably less than 0.5 kpc distant, but outside the Local Bubble.

The remainder of Table 1 lists geometric results and derived gas properties of each HISA feature. The first number in each range corresponds to a value on the left edge of the strip, the second to the right edge. Gas properties are computed for the $p = 1, f_n = 1$ case, which represents a lower limit on feature mass, and for the maximum mass obtainable with $f_n = 0.01$ and other allowed parameters. These two cases give essentially the full range of properties consistent with present constraints: $f_n < 0.01$ is allowed for the first two features, but only if T_S approaches 2.7 K, which may be prevented by cosmic ray heating within these objects. If we require $T_S > 7$ K, then $f_n \geq 0.03$ for two of the three features, and $f_n \geq 0.01$ for the third. The large gas mass ranges are a consequence of the poor constraints on f_n.

5.2. Individual Features

5.2.1. Perseus Complex

This intricate, amorphous feature is possibly the warmest of the three, and is certainly the most massive, with at least 30 $M_\odot$ of total gas in the $6' \times 6'$ ON box in Fig. 2. The mass of the entire complex, defined arbitrarily as the set of contiguous HISA within 0.5° of the ON box, is easily 10 times that within the box. In addition, the detection of ^{12}CO emission indicates f_n is less than unity, perhaps much less, which requires the feature to be even more massive and T_S to be

lower. If the gas is extremely cold, dense, and mostly molecular, the gas mass of the whole complex feature may lie in the $10^4 - 10^5$ $M_\odot$ range, making it a giant molecular cloud. In this same regime, simplistic Jeans mass calculations suggest the object is gravitationally bound.

Other dark complexes and concentrations of Perseus-velocity HISA are found over the currently completed area of our survey (§3.1). Together, they may represent a significant amount of the interstellar matter in the spiral arm.

5.2.2. Perseus Globule

This dark, compact feature on the outskirts of the larger HISA complex is less massive than the larger structure, and perhaps also colder and more opaque. The globule is unresolved spatially, and probably unresolved spectrally. In either case, its true opacity is diluted in our data, and its T_S is lower and its density is greater than each appears.

Might this object and others like it be gravitationally bound? Neglecting magnetic fields and other nonthermal pressure sources, the Jeans mass (Binney & Tremaine 1987) is

$$M_J \simeq \frac{\pi}{6}\left(\frac{\gamma\,\pi\,k\,T_S}{G\,\mu}\right)^{3/2}\left(\frac{1}{\mu\,n_{tot}}\right)^{1/2} , \tag{10}$$

where μ is the mean particle mass in grams and γ is the gas polytropic exponent. Assuming pure hydrogen, $\mu = (2 - f_n)\,m_H$. We use $\gamma = 5/3$, the ideal monatomic value, which may be an overestimate for the real gas.

For this feature, the total mass of the globule exceeds M_J by a factor of ~ 9 for the 2.7 K solution listed in Table 1, but $M_{tot}/M_J \sim 0.5$ if $T_S = 7$ K. If the globule diameter is less than the CGPS resolution, the possibility of gravitational collapse exists without the need for extremely cold gas. However, the current nondetection of CO is consistent with the warmest, least massive, $f_n = 1$ solution, which gives a much lower fraction of $M_{tot}/M_J < 10^{-3}$. Additional observations are clearly needed to determine the dynamical state of this object.

5.2.3. Local Filament

This small, faint, filamentary Local feature has the lowest upper limit to T_S and may have the lowest opacity; it is certainly the least massive of the three example features. A firm coincidence of ^{12}CO emission would lower the T_S ceiling further. M_{tot}/M_J ranges from 10^{-6} at the warm, low-mass end to 0.3 at the cold, high-mass end, indicating the feature is not gravitationally bound. Exceeding M_J may be possible in this case if the feature is significantly unresolved, but the visible structure makes this appear less likely than it does for the globule.

5.3. General Characteristics

Do all HISA features have similar properties, despite their varying sizes and appearances?

The large range of allowed f_n for the three HISA features we have discussed gives them a common parameter set, presenting the possibility all of them having similar T_S and τ values. This may change with better constraints on f_n and other parameters. The common zone is bounded by the $p = 1$ curve for the globular feature on the bottom, the Local filament's $f_n = 1$ strip edge on the right side, and by the $T_S \geq 2.73$ K (or 7 K) and $\tau \leq 10$ limits on the left and top. These suggest $3 < T_S < 20$ K and $0.8 < \tau < 10$ if all HISA features are essentially similar.

However, we have no a priori reason to expect the properties of all HISA features to be identical. Certainly their appearances vary considerably, from dark and compact to faint and diffuse, with many different shapes and structures. A more direct indication of varying properties is given by the comparison of the heart of the Perseus complex with the globule on its periphery. For the same f_n, these features may have similar T_S and τ values, but only if their p fractions differ by 0.3 or more, which is not easy to explain if they are physically associated. Either the globule is significantly closer, or it is significantly more opaque. The latter possibility seems more likely, given the association of globule and complex suggested by the morphology of HISA and 60 μm emission in the vicinity.

Deciding this issue requires tighter constraints from additional observations, which we are pursuing in a followup investigation. For now, the possibility of "canonical" HISA properties remains open.

6. Conclusions

We have presented a new view of cold H I outside the Solar circle obtained with high resolution images of self-absorption over a large area of the Galactic plane. We find HISA features to be numerous and complex, exhibiting a wide range of sizes, structures, and contrasts against the background H I emission. The majority of these features can only be investigated with wide-field synthesis mapping efforts like the Canadian Galactic Plane Survey; even so, some HISA appears unresolved and undersampled and will require more detailed observations to be explored properly.

HISA observations are underutilized in the investigation of cold H I gas. Though identifiable HISA clouds represent only the subset of cold H I which has sufficiently bright background emission and cannot be explained as gaps in the emitting H I, they are nonetheless sufficiently common to give a more complete view of such clouds than that provided by absorption studies toward continuum sources.

More problematic is the determination of physical properties of the gas in HISA features. We have outlined a new method of addressing this issue, which also shows more clearly how these

properties are related to each other. Though currently limited by a degree of uncertainty in its own input parameters, especially the fraction of gas which is atomic, this alternative approach holds considerable promise if employed with additional observations, e.g., column densities of molecular species.

Finally, and perhaps most significantly, our survey demonstrates a considerable disagreement between maps of HISA and ^{12}CO, with only a fraction of HISA features containing detected CO, and vice-versa. A few previous single dish surveys have indicated the HISA-CO association is only partial, but the higher resolution of the CGPS demonstrates this result conclusively. We must now call into question the commonly held picture of HISA arising primarily from trace amounts of H I in molecular clouds, unless the CO itself is an inadequate probe of H_2. Either way, the traditional view of cold interstellar matter requires reexamination.

We recommend a number of further observations to address the issues raised herein. First, our CGPS results suggest other wide-field synthesis surveys of H I are necessary for a more complete view of HISA in the Galaxy; a fourth-quadrant survey is already underway (Dickey et al. 1999). Second, sub-arcminute resolution imaging of H I, as well as CO and dust, is needed to resolve some globular features, and to assess the small-scale structure of other HISA. High resolution is very important for constraining the physical parameters of these features. Even more critical to our analysis technique is the determination of H_2 content, which may be approached through observations of various molecular species. While many HISA features appear to lack ^{12}CO emission, this needs to be assessed with higher-sensitivity ^{12}CO observations.

It is a pleasure to thank J. Dickey for a number of helpful comments and suggestions regarding the manuscript. We are also very grateful to E. Donovan for additional comments on magnetic fields. The Canadian Galactic Plane Survey (CGPS) is a Canadian project with international partners. The CGPS is described in Taylor et al. (2000), with additional information available online at the address www.ras.ucalgary.ca/CGPS. The Dominion Radio Astrophysical Observatory is operated as a national facility by the National Research Council of Canada. The CGPS is supported by a grant from the Natural Sciences and Engineering Research Council of Canada.

REFERENCES

Allen, R. J., & Lequeux, J. 1993, ApJ, 410, L15

Allen, R. J., Le Bourlot, J., Lequeux, J., Pineau des Forêts, G., & Roueff, E. 1995, ApJ, 444, 157

Baker, P. L., & Burton, W. B. 1979, A&AS, 35, 129

Bania, T. M., & Lockman, F. J. 1984, ApJS, 54, 513

Binney, J., & Tremaine, S. 1987, *Galactic Dynamics* (Princeton: Princeton University Press)

Burton, W. B., Liszt, H. S., & Baker, P. L. 1978, ApJ, 219, L67

Cao, Y., Terebey, S., Prince, T. A., & Beichman, C. A. 1997, ApJS, 111, 387

Dame, T. M., Ungerechts, H., Cohen, R. S., de Geus, E., Grenier, I. A., May, J., Murphy, D. C., Nyman, L. A., & Thaddeus, P. 1987, ApJ, 322, 706

Dickey, J. M., & Lockman, F. J. 1990, ARA&A, 28, 215

Dickey, J. M., McClure-Griffiths, N. M., Gaensler, B., Green, A., Haynes, R., & Wieringa, M. 1999, ASP Conf. Ser. 168, *New Perspectives on the Interstellar Medium*, eds. A. R. Taylor, T. L. Landecker, & G. Joncas, p. 27

Faison, M. D., Goss, W. M., Diamond, P. J., & Taylor, G. B. 1998, AJ, 116, 2916

Feldt, C. 1993, A&A, 276, 531

Feldt, C., & Wendker, H. J. 1993, A&AS, 100, 287

Garwood, R. W., & Dickey, J. M. 1989, ApJ, 338, 841

Goerigk, W., Mebold, U., Reif, K., Kalberla, P. M. W., & Velden, L. 1983, A&A, 120, 63

Hasegawa, T., Sato, F., & Fukui, Y. 1983, AJ, 88, 658

Heeschen, D. J. 1955, ApJ, 121, 569

Heiles, C. 1997, ApJ, 481, 193

Heyer, M. H., Brunt, C., Snell, R. L., Howe, J. E., Schloerb, F. P., & Carpenter, J. M. 1998, ApJS, 115, 241

Jacq, T., Baudry, A., & Walmsley, C. M. 1988, A&A, 207, 145

Knapp, G. R. 1974, AJ, 79, 527

Kulkarni, S. R., & Heiles, C. 1988, in *Galactic and Extragalactic Radio Astronomy*, eds. G. L. Verschuur, & K. I. Kellermann (New York: Springer-Verlag), p. 95

Landecker, T. L., Dewdney, P. E., Burgess, T. A., Gray, A. D., Higgs, L. A., Hoffmann, A. P., Hovey, G. J., Karpa, D. R., Lacey, J. D., Prowse, N., Purton, C. R., Roger, R. S., Willis, A. G., Wyslouzil, W., Routledge, D., & Vaneldik, J. F. 1999, A&A, submitted

Levinson, F. H., & Brown, R. L. 1980, ApJ, 242, 416

Liszt, H. S., Burton, W. B., & Bania, T. M. 1981, ApJ, 246, 74

Loinard, L., & Allen, R. J. 1998, ApJ, 499, L227

McCutcheon, W. H., Shuter, W. L. H., & Booth, R. S. 1978, MNRAS, 185, 755

Meyer, D. M., & Lauroesch, J. T. 1999, ApJ, 520, L103

Meyerdierks, H., & Heithausen, A. 1996, A&A, 313, 929

Mihalas, D., & Binney, J. 1981, *Galactic Astronomy: Structure and Kinematics* (New York: Freeman)

Montgomery, A. S., Bates, B., & Davies, R. D. 1995, MNRAS, 273, 449

Normandeau, M. 1999, AJ, 117, 2440

Peters, W. L., & Bash, F. N. 1987, ApJ, 317, 646

Pöppel, W. G. L., Marronetti, P., & Benaglia, P. 1994, A&A, 287, 601

Reach, W. T., Koo, B.-C., & Heiles, C. 1994, ApJ, 429, 672

Rohlfs, K., Braunsfurth, E., & Mebold, U. 1972, AJ, 77, 711

Roberts, W. W. 1972, ApJ, 173, 259

Spitzer, L. 1978, *Physical Processes in the Interstellar Medium* (New York: Wiley & Sons)

Taylor, A. R., Dougherty, S. M., Gibson, S. J., Peracaula, M., Landecker, T. L., Higgs, L., Gray, A., Willis, T., Wallace, B., & Knee, L. 2000, AJ, submitted

Turner, B. E. 1988, in *Galactic and Extragalactic Radio Astronomy*, eds. G. L. Verschuur, & K. I. Kellermann (New York: Springer-Verlag), p. 154

van der Werf, P. P., Dewdney, P. E., Goss, W. M., & Vanden Bout, P. A. 1989, A&A, 216, 215

van der Werf, P. P., Goss, W. M., & Vanden Bout, P. A. 1988, A&A, 201, 311

Wendker, H. J., & Wrigge, M. 1996, A&A, 305, 592

Wolkovitch, D., Langer, W. D.; Goldsmith, P. F.; & Heyer, M. 1997, ApJ, 477, 241

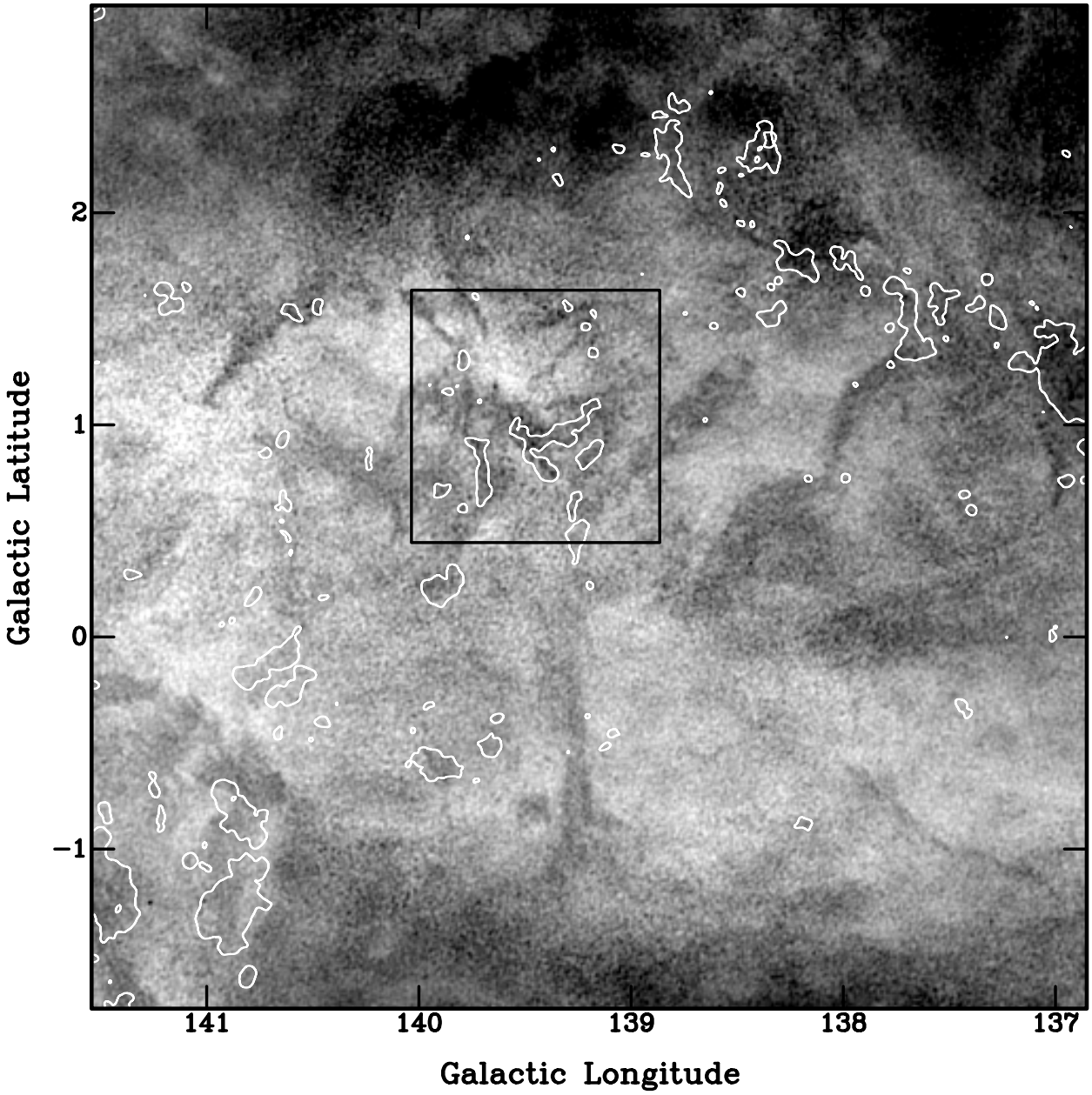

Fig. 1.— One CGPS H I 21cm emission field rich in self-absorption features. This channel map has an LSR velocity of -41 km s^{-1}, characteristic of gas in the Perseus spiral arm. Brightness temperatures displayed range from 40 K (black) to 130 K (white). ^{12}CO emission from Heyer et al. (1998) is marked with a white contour at 1 K. The black box marks the area of Fig. 2.

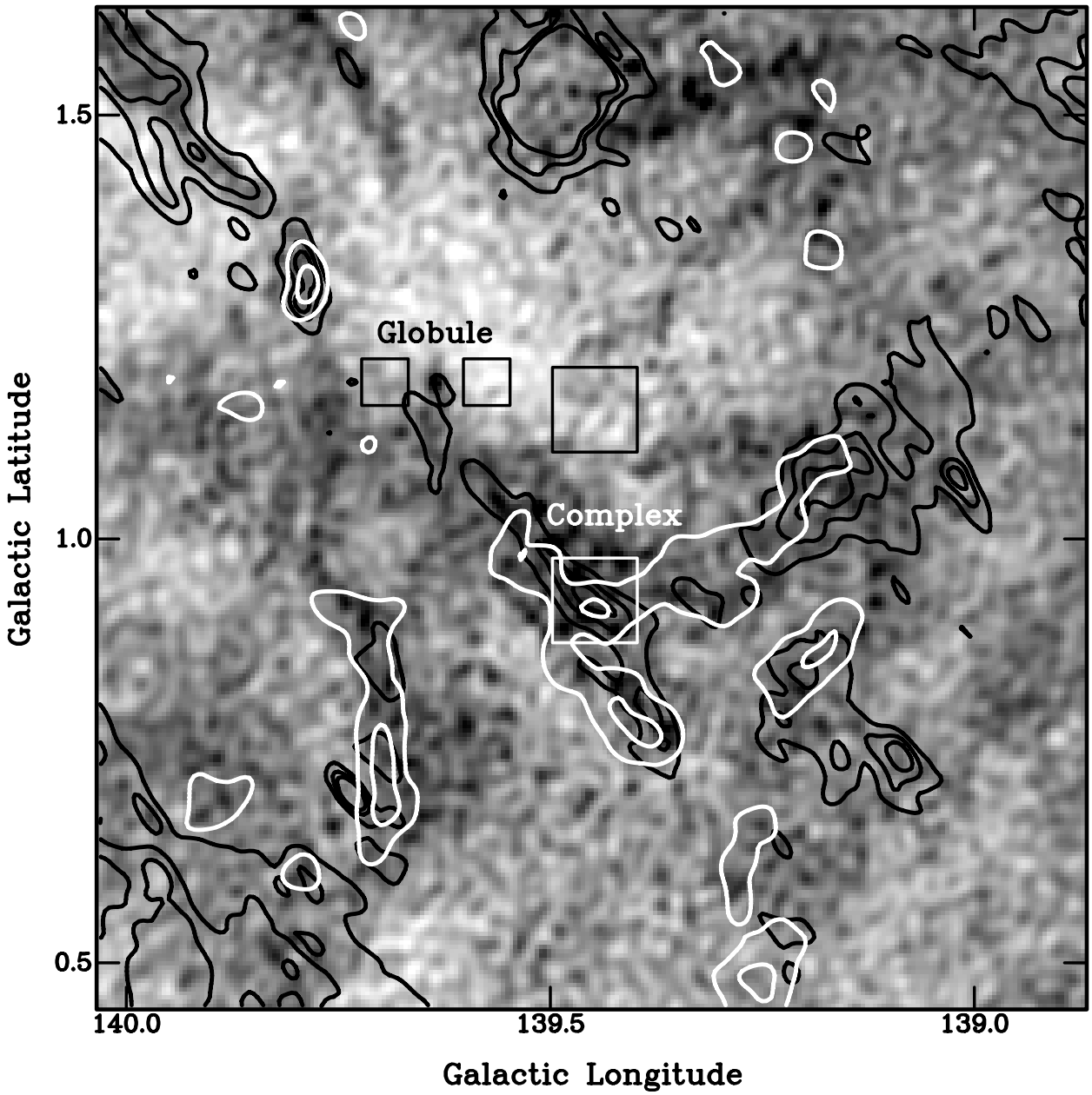

Fig. 2.— Enlarged view of several HISA features shown in Fig. 1. White contours trace CO emission levels of 1, 3, & 5 K. Black contours trace 60 μm emission at 15, 17, & 19 MJy sr^{-1} levels. ON and OFF spectra for part of the extended HISA complex (§3.3.1) were extracted from the large white and black boxes respectively. OFF spectra for the HISA globule (§3.3.2) were averaged from the two small black boxes, with a single-pixel ON spectrum taken from the darkest part of the feature between them.

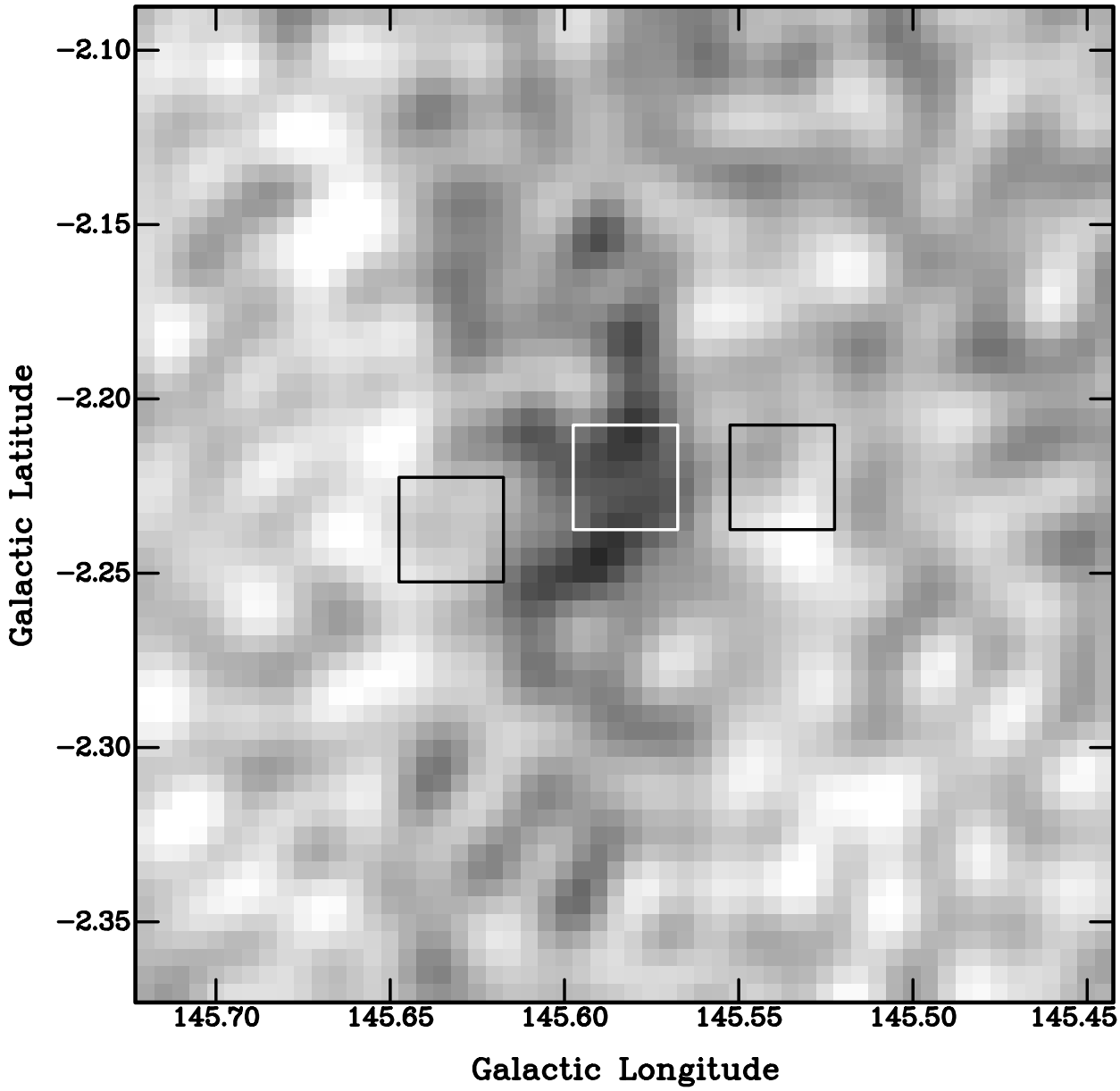

Fig. 3.— Example of a HISA feature at Local arm velocities, here 0 $\mathrm{km\,s^{-1}}$. Brightness temperatures displayed range from 55 K (black) to 90 K (white). No dust counterparts were found, and available CO data has insufficient angular resolution to show molecular gas on these scales. ON and OFF spectra were extracted from the $2' \times 2'$ white and black boxes, respectively.

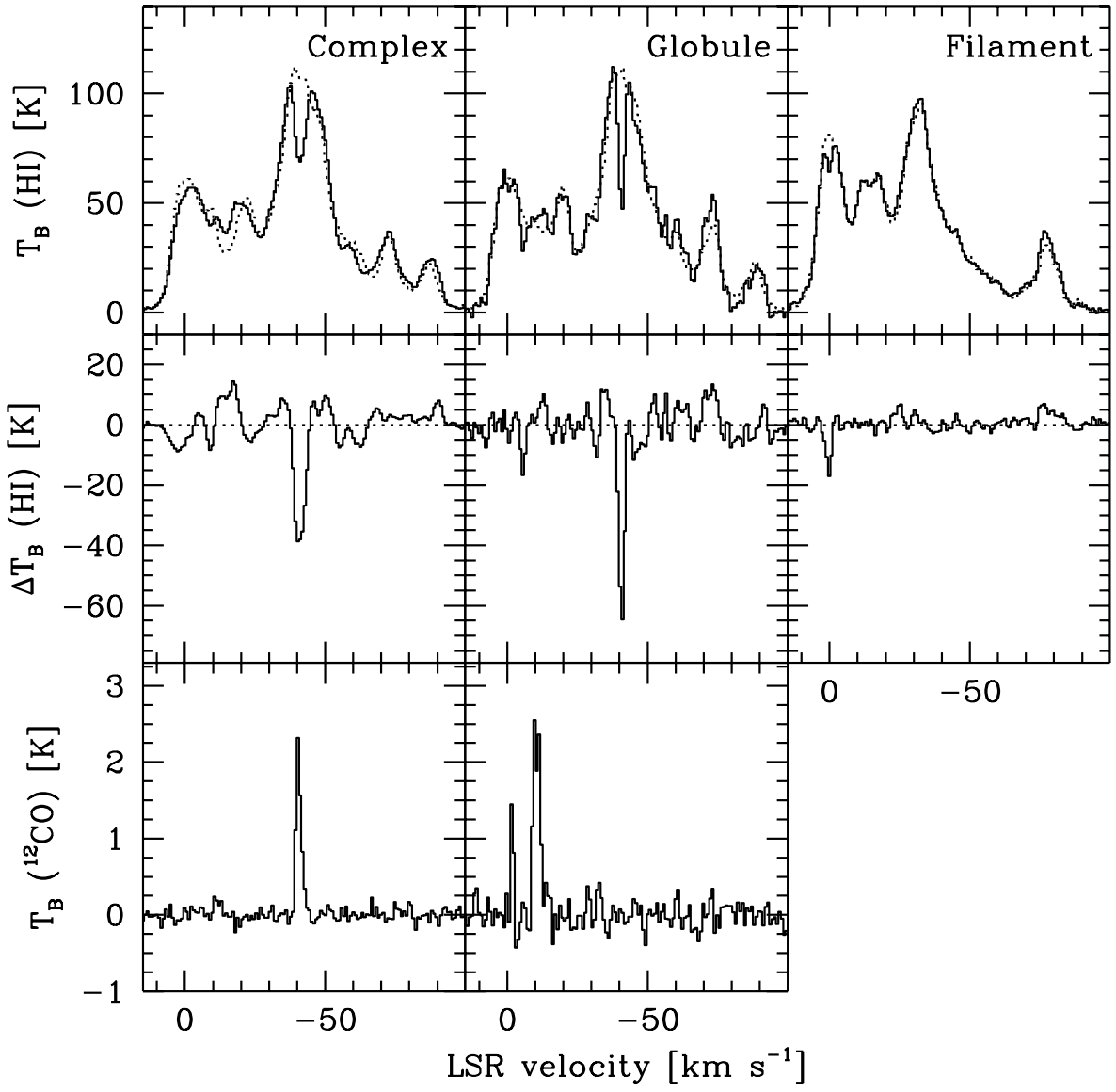

Fig. 4.— Spectra extracted from the $6' \times 6'$ white box (*left*) and individual sightline (*center*) in Fig. 2 and from the white box in Fig. 3 (*right*). Shown are the H I ON (*solid*) and OFF (*dotted*) spectra (*top*), H I difference spectra (*center*), and ^{12}CO ON spectra where high-resolution data are available (*bottom*). For a simple Galactic rotation model, the velocity axis has distance in increasing from left to right, with Local gas near 0 km s^{-1}, Perseus gas near -40 km s^{-1}, and Outer arm gas near -80 km s^{-1}.

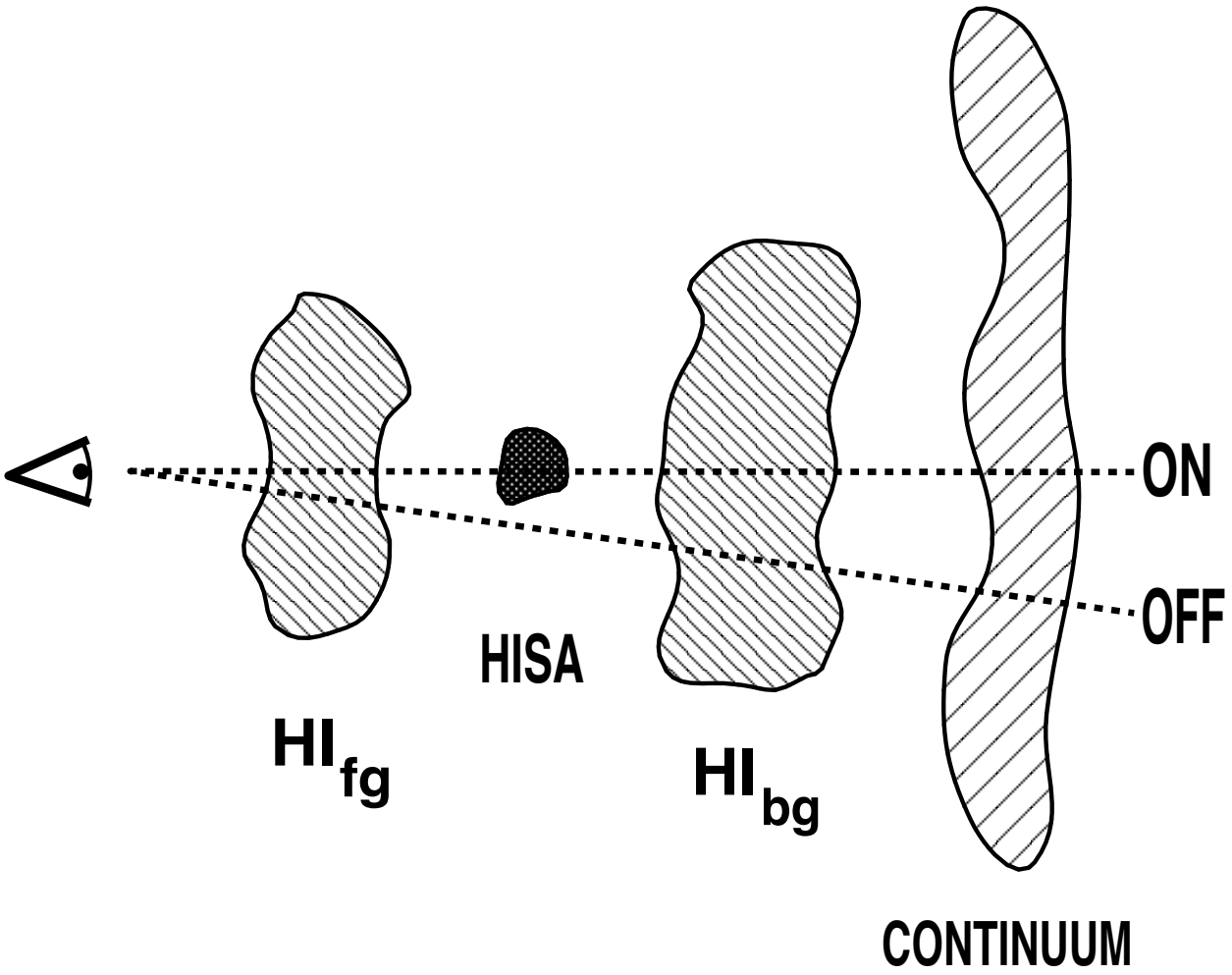

Fig. 5.— Schematic view of 4-component radiative transfer geometry, showing ON and OFF sightlines with respect to the HISA cloud, foreground and background H I emission, and background continuum emission. All H I clouds must share the HISA radial velocity to participate in the transfer relationship. Though drawn separately, the two H I emission clouds may be merged into a single cloud enveloping the HISA in a special case of this geometry, which has the same solution (Eq. [4]).

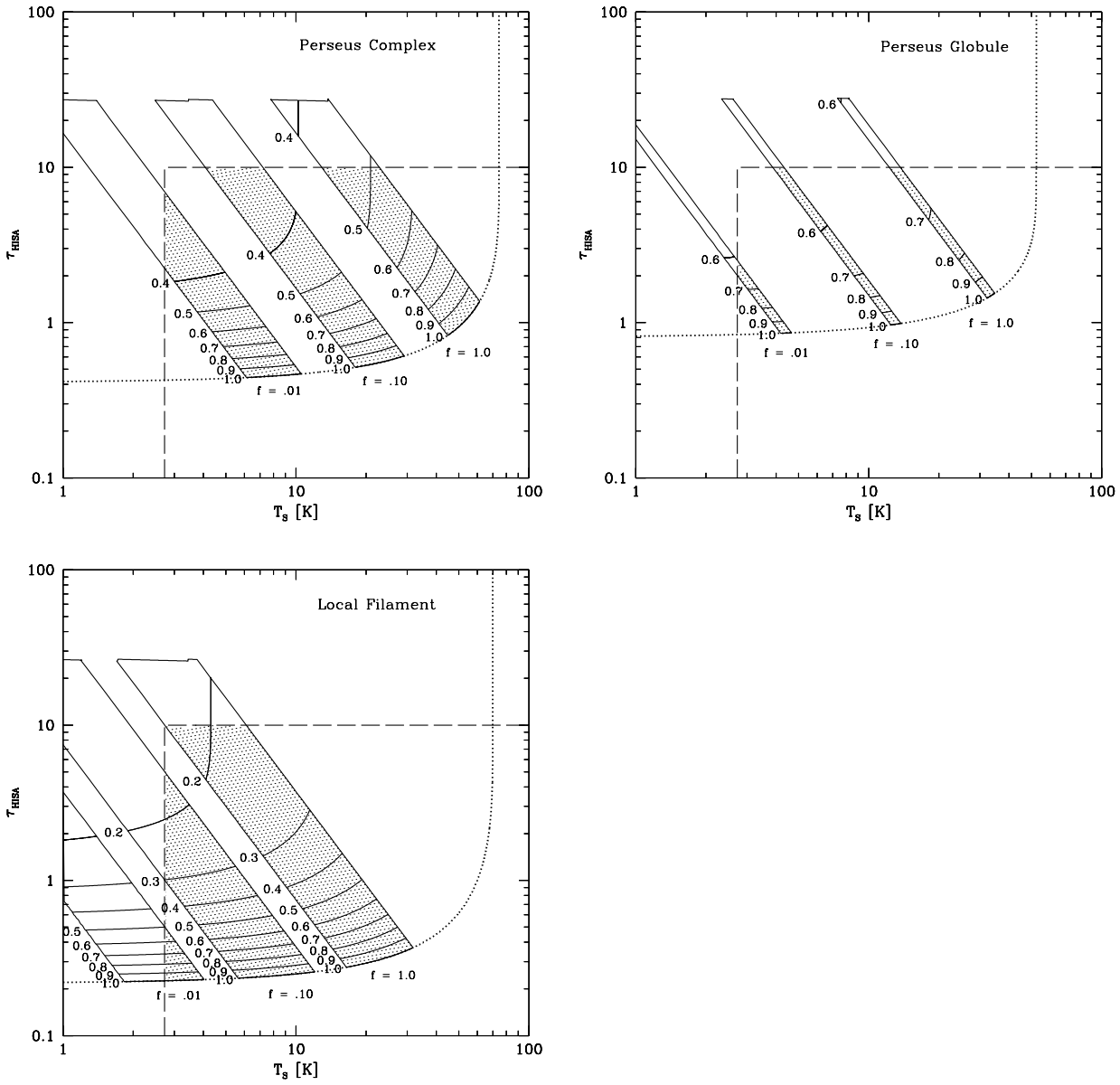

Fig. 6.— Constraints on T_S and τ values for features discussed in the text: (a) Perseus complex; (b) Perseus globule; (c) Local filament. In each case, the shaded areas shows the solution sets permitted by the available constraints for a given f_n, with curves of constant p marked. For the $p = 1$ case, the full (T_S, τ) relation is shown as a dotted line. The dashed line marks two external constraints on T_S and τ. We presume T_S cannot be colder than the 2.7 K cosmic microwave background, and find optical depths of more than a few are excluded by line profile shapes. The strip widths reflect uncertainties in feature geometric thickness Δs.

Table 1. HISA Feature Properties

			Perseus Complex	Perseus Globule	Local Filament
Input	T_{ON}	[K]	69	47	65
	T_{OFF}	[K]	107	112	82
	T_C	[K]	5.4	5.4	4.9
	Δv	$[\mathrm{km\,s^{-1}}]$	4.5	2.5	2.5
	Ω	$[\mathrm{arcmin}^2]$	6×6	1×1	2×2
	θ_s	$[']$	$2 - 5$	1	1
	d	[kpc]	$2.0 - 2.5$	$2.0 - 2.5$	$0.1 - 0.5$
Geometry	Δs	[pc]	$1.2 - 3.6$	$0.58 - 0.73$	$0.029 - 0.15$
	Area	$[\mathrm{pc}^2]$	$12 - 19$	$0.34 - 0.53$	$0.0034 - 0.085$
	Volume	$[\mathrm{pc}^3]$	$14 - 68$	$0.20 - 0.39$	$0.00010 - 0.013$
Gas Properties ($p = f_n = 1$)	T_S	[K]	$45 - 61$	$32 - 35$	$16 - 32$
	τ		$0.83 - 1.37$	$1.43 - 1.54$	$0.28 - 0.37$
	N_{HISA}	$[10^{20}\ \mathrm{cm}^{-2}]$	$3.2 - 7.3$	$2.2 - 2.6$	$0.22 - 0.56$
	n_{HISA}	$[\mathrm{cm}^{-3}]$	$89 - 65$	$124 - 115$	$243 - 126$
	M_{HISA}	$[\mathrm{M}_\odot]$	$31 - 111$	$0.60 - 1.09$	$0.00059 - 0.038$
($f_n = 0.01$, Maximum Total Mass)	T_S	[K]	2.7	2.7	2.7
	τ		7.0	2.5	0.49
	N_{HISA}	$[10^{20}\ \mathrm{cm}^{-2}]$	1.7	0.33	0.066
	n_{HISA}	$[\mathrm{cm}^{-3}]$	15	15	15
	M_{HISA}	$[\mathrm{M}_\odot]$	26	0.14	0.0045
	N_{tot}	$[10^{20}\ \mathrm{cm}^{-2}]$	170	33	6.6
	n_{tot}	$[\mathrm{cm}^{-3}]$	1500	1500	1500
	M_{tot}	$[\mathrm{M}_\odot]$	5200	28	0.89